

# **Somatostatin, an *In Vivo* Binder to A $\beta$ Oligomers, Binds to $\beta$ PFO<sub>A $\beta$ (1-42)</sub> Tetramer**

Eduard Puig,<sup>1,2\*</sup> James Tolchard,<sup>2</sup> Antoni Riera,<sup>1,3\*</sup> Natàlia Carulla<sup>1,2\*</sup>

<sup>1</sup>Institute for Research in Biomedicine (IRB Barcelona), The Barcelona Institute of Science and Technology (BIST), Baldiri Reixac 10, 08028 Barcelona, Spain

<sup>2</sup>CBMN (UMR 5248), University of Bordeaux – CNRS – IPB, Institut Européen de Chimie et Biologie, 2 rue Escarpit, 33600, Pessac, France

<sup>3</sup>Departament de Química Inorgànica i Orgànica. Universitat de Barcelona, Martí i Franqués 1, 08028, Barcelona, Spain

\*Corresponding authors:

Eduard Puig, e-mail: [eduard.puig@irbbarcelona.org](mailto:eduard.puig@irbbarcelona.org)

Natàlia Carulla, e-mail: [natalia.carulla@gmail.com](mailto:natalia.carulla@gmail.com)

## Abstract

Somatostatin (SST14) is strongly related to Alzheimer's disease (AD), as its levels decline during aging, it regulates the proteolytic degradation of the amyloid beta peptide ( $A\beta$ ), and it binds to  $A\beta$  oligomers *in vivo*. Recently, the 3D structure of a membrane-associated  $\beta$ -sheet pore forming tetramer ( $\beta$ PFO $_{A\beta(1-42)}$  tetramer) has been reported. Here we show that SST14 binds selectively to the  $\beta$ PFO $_{A\beta(1-42)}$  tetramer with an a  $K_D$  of  $\sim 40 \mu\text{M}$  without binding to monomeric  $A\beta(1-42)$ . Specific NMR chemical shift perturbations, observed during titration of SST14, define a binding site in the  $\beta$ PFO $_{A\beta(1-42)}$  tetramer and are in agreement with a 2:1 stoichiometry determined by both native MS and ITC. These results enabled us to perform driven docking and model the binding mode for the interaction. The present study provides additional evidence on the relation between SST14 and the amyloid cascade, as well as positions the  $\beta$ PFO $_{A\beta(1-42)}$  tetramer as a relevant aggregation form of  $A\beta$  and as a potential target for AD.

## Introduction

Increased levels of amyloid beta peptide (A $\beta$ ) and deposition of amyloid fibrils in neuronal cells constitute a critical part of the etiopathogenesis in Alzheimer's disease (AD).<sup>1,2</sup> A $\beta$  originates from the sequential cleavage of the amyloid precursor protein (APP) by the  $\beta$ -secretase in the extracellular space and the  $\gamma$ -secretase in the transmembrane domain.<sup>3</sup> In solution, this hydrophobic peptide aggregates in a nucleation-dependent manner into soluble oligomers<sup>4</sup> that gradually increase in molecular-weight until insoluble fibrils are formed<sup>5-8</sup>. The presence of amyloid fibrils in the extracellular space has inevitably drawn research interest in A $\beta$  peptides to this location. However, the fact that A $\beta$ 's origin lies within APP, a transmembrane protein,<sup>9</sup> together with numerous reported work of A $\beta$  interacting with the cellular membrane,<sup>10-15</sup> strongly suggests this environment as an alternative location for A $\beta$  accumulation and aggregation.

We have previously studied the aggregation of A $\beta$  within detergent micelles to mimic the membrane environment and reported the preparation<sup>16</sup> and the three-dimensional (3D) structure<sup>17</sup> of a membrane-associated  $\beta$ -sheet pore forming tetramer ( $\beta$ PFO<sub>A $\beta$ (1-42)</sub> tetramer) (Figure S1). Interestingly, the formation of this oligomer was specific for A $\beta$ (1-42), the variant most related to AD but not A $\beta$ (1-40) which is the variant most abundant in the brain.  $\beta$ PFO<sub>A $\beta$ (1-42)</sub> tetramer comprises a  $\beta$ -sheet core formed by six  $\beta$ -strands. Molecular dynamics showed that when  $\beta$ PFO<sub>A $\beta$ (1-42)</sub> tetramer incorporated into lipid bilayers and water molecules were able to permeate the membrane through the hydrophilic edges of the  $\beta$ -sheet core tetramer. This work not only represented the resolution of the first 3D structure of an A $\beta$  oligomer but also the definition of a new mechanism of membrane disruption that could explain the neurotoxic activity of A $\beta$  oligomers in the context of AD.

The screening of potential interactors constitutes an essential step to better understand the function of A $\beta$  and its implication in AD. Schmitt-Ulms *et al.* recently performed an extensive

screening of proteins that bound to A $\beta$  oligomers in human brain extracts.<sup>18</sup> From over 50 proteins detected, somatostatin (SST14) stood out for delaying A $\beta$  aggregation and binding specifically to A $\beta$  oligomers. To the best of our knowledge, the aforementioned work represents the largest A $\beta$  monomeric and oligomeric *in vivo* interactome performed so far. The authors suggested that further investigations should be performed to improve the understanding of the SST14-A $\beta$  interaction. In the present work, we used well established biophysical techniques to assess whether the specific A $\beta$  oligomer binder, somatostatin-14 (SST14) bound to the  $\beta$ PFO<sub>A $\beta$ (1-42)</sub> tetramer.

SST14 is a cyclic tetradecapeptide that is produced in neuroendocrine cells in the hypothalamus as well as in other tissues, including pancreas, intestinal tract and regions of the central nervous system.<sup>19,20</sup> In a clinical context, SST14 is the neuropeptide most highly depleted in both the brain and cerebrospinal fluid (CSF) of AD patients.<sup>21,22</sup> The relation to AD was further described by the work of Saido *et al.* as they found that SST14 regulates the metabolism of A $\beta$  in the brain through the modulation of neprilysin which catalyses its proteolytic degradation.<sup>23</sup> Moreover, a positive correlation between SST14 and A $\beta$ (1-42) levels was established in the CSF of elderly patients with mild cognitive impairment.<sup>24</sup> Undoubtedly, previous work in the literature has established a strong link between SST14, A $\beta$  and AD. Therefore, studying the potential interaction between SST14 and  $\beta$ PFO<sub>A $\beta$ (1-42)</sub> tetramer could deliver evidence to better understand the role of SST14 in the context of AD and point towards the relevance of  $\beta$ PFO<sub>A $\beta$ (1-42)</sub> tetramer in a biological context.

## Results

### SST14 coelutes with $\beta$ PFO<sub>A $\beta$ (1-42)</sub> tetramers

We initially relied on size exclusion chromatography (SEC)<sup>25-27</sup> to characterize the potential interaction between SST14 and  $\beta$ PFO<sub>A $\beta$ (1-42)</sub> tetramer in a membrane mimicking environment. As control samples, we followed the evolution of  $\beta$ PFO<sub>A $\beta$ (1-42)</sub> tetramer formation and SST14 independently, following its incubation in the dodecyl phosphocholine (DPC) solution used as a membrane mimicking environment. Analysis of both samples showed that  $\beta$ PFO<sub>A $\beta$ (1-42)</sub> tetramers and SST14 eluted, respectively, at 13.5 mL and 17.5 mL (Supporting information; Figure S2A, B). In the case of the SST14 sample, its evolution over time revealed the appearance of wide peaks near the void volume, which were attributed to aggregated forms as previously reported for this peptide.<sup>28</sup> Coincubation of A $\beta$ (1-42) with SST14 under conditions that lead to  $\beta$ PFO<sub>A $\beta$ (1-42)</sub> tetramer formation resulted in an increase of 65% of the area under the peak assigned to  $\beta$ PFO<sub>A $\beta$ (1-42)</sub> tetramers (Figure 1A). Such a change could be explained either due to an increase in the formation of  $\beta$ PFO<sub>A $\beta$ (1-42)</sub> tetramer or the binding of SST14. Interestingly, we did not observe precipitates when both peptides were coincubated suggesting that the interaction between them increased the stability of SST14 in a membrane-mimicking environment. To assess whether binding occurred specifically during  $\beta$ PFO<sub>A $\beta$ (1-42)</sub> tetramer formation, we first incubated A $\beta$ (1-42) alone for 24 h under conditions that lead to  $\beta$ PFO<sub>A $\beta$ (1-42)</sub> tetramer formation and then added SST14. Analysis of this sample by SEC resulted in a 20% increase of the area under the peak assigned to  $\beta$ PFO<sub>A $\beta$ (1-42)</sub> tetramer (Supporting information, Figure S2D). This result suggested that SST14 binding was not exclusively occurring during  $\beta$ PFO<sub>A $\beta$ (1-42)</sub> tetramer formation but also when putting in contact the two binding partners after the oligomer was assembled.

## SST14 interacts with the A $\beta$ (1-42) tetramer at a 2:1 ratio

To further study the interaction between  $\beta$ PFO<sub>A $\beta$ (1-42)</sub> tetramer and SST14, we used isothermal titration calorimetry (ITC) to measure the heat exchange and obtain information about the energetic profile of the binding event. Titration of SST14 to the  $\beta$ PFO<sub>A $\beta$ (1-42)</sub> tetramer showed an exothermic interaction with a  $K_D$  of  $\sim 40 \mu\text{M}$  and a stoichiometry of approximately 2:1 (SST14 to  $\beta$ PFO<sub>A $\beta$ (1-42)</sub> tetramer) (Figure 1B, C). Such a binding ratio would indeed be in agreement with the symmetric structure of the  $\beta$ PFO<sub>A $\beta$ (1-42)</sub> tetramer. However, we could not exclude the possibility of SST14 interacting with remaining monomeric A $\beta$ (1-42) in the sample.

To better understand the specificity and stoichiometry of the interaction we analyzed the sample using native mass spectrometry (MS). This technique uses non-denaturing conditions to prepare the sample and soft ionization methods (such as electrospray ionization (ESI)) to preserve the non-covalent interactions within ( $\beta$ PFO<sub>A $\beta$ (1-42)</sub> tetramer) and between ( $\beta$ PFO<sub>A $\beta$ (1-42)</sub> tetramer-SST14) molecular complexes.<sup>29,30</sup> To prepare the  $\beta$ PFO<sub>A $\beta$ (1-42)</sub> tetramer sample for MS analysis, we used lauryldimethylamine *N*-oxide (LDAO) instead of DPC to mimic the membrane environment as this detergent also supports  $\beta$ PFO<sub>A $\beta$ (1-42)</sub> tetramer formation and is compatible with MS analysis.<sup>31</sup> Direct infusion of the resulting sample using nanoESI-MS delivered a clean spectrum displaying four consecutive charge states for the tetramer (+3, +4, +5 and +6) confirming that it was the major species in the sample (Figure 2A; Supporting information, Table S2). Infusion of a  $\beta$ PFO<sub>A $\beta$ (1-42)</sub> tetramer sample prepared in the presence of SST14 revealed consecutive charge states that were assigned to one (+3, +4 and +5) and two (+4, +5 and +6) SST14 molecules bound to the  $\beta$ PFO<sub>A $\beta$ (1-42)</sub> tetramer (Figure 2B; Supporting information, Table S2). Both ITC (Figure 1C) and native MS (Figure 2B) data pointed towards a 2:1 ratio for SST14 and  $\beta$ PFO<sub>A $\beta$ (1-42)</sub> tetramer interaction. Moreover, we did not observe any consecutive charge states corresponding to monomeric A $\beta$ (1-42) bound to one or two SST14

molecules in agreement with SST14 binding specifically to oligomeric forms of A $\beta$  (Supporting information; Figure S3, Table S1).

### **SST14 binds to the flexible edges of the A $\beta$ (1-42) tetramer**

The results obtained by SEC indicated that the binding event was stable over 24 h in the membrane-mimicking environment (Supporting information, Figure S2C), which encouraged us to further study the interaction by solution NMR. We therefore decided to pursue a deeper characterization by titrating SST14 into a  $^{15}\text{N}$ - $\beta\text{PFO}_{\text{A}\beta(1-42)}$  tetramer sample and perform 2D [ $^1\text{H}$ ,  $^{15}\text{N}$ ]-SOFAS-HMQC experiments over time. The  $\beta\text{PFO}_{\text{A}\beta(1-42)}$  tetramer consists of a six-stranded  $\beta$ -sheet comprising two types of A $\beta$ (1-42) subunits referred to orange and green, respectively (Supporting information, Figure S1). The orange subunit contributes with two  $\beta$ -strands ( $\beta$ 1 and  $\beta$ 2) and the green subunit contributes with one  $\beta$ -strand ( $\beta$ 3) and a small  $\alpha$ -helix ( $\alpha$ 1).<sup>17</sup>

The spectrum for  $\beta\text{PFO}_{\text{A}\beta(1-42)}$  tetramer displayed a well-dispersed set of signals as previously reported for this sample (Figure 3).<sup>16</sup> Upon addition of SST14 to the NMR sample, several changes in chemical shifts were observed in the resulting spectrum indicating that SST14 bound to  $\beta\text{PFO}_{\text{A}\beta(1-42)}$  tetramer. Indeed, specific shift changes in residues V12, F20, V24 G29, V40 and A42 of the orange subunit and in residues V12, V18, A21, E22, D23, G29, I41 and A42 of the green subunit of the  $\beta\text{PFO}_{\text{A}\beta(1-42)}$  tetramer were observed (Figure 4A; Supporting information, Figure S4; Source data 1). Chemical Shift Perturbations (CSPs) were considered significant if the values were greater than one standard deviation ( $\sigma$ ) of the Euclidean chemical shift change represented as a grey dashed line (Figure 4A, Source data 1).<sup>32</sup> Both the observation of smooth peak migrations between the free and bound states, and the derivation of  $k_{\text{off}}$  rates using the maximum change in chemical shift, indicated that somatostatin binding occurred in the fast-exchange regime (Figure 3C).<sup>32,33</sup>  $K_{\text{D}}$  rates were determined for each clearly tractable residue by fitting the change in chemical shift as a function of the ligand

concentration. The tightest binding residues (Y10, F20) exhibited  $K_D$ 's of  $\sim 35$  and  $\sim 52$   $\mu\text{M}$ , respectively.

The CSPs induced by SST14 were represented in the  $\beta\text{PFO}_{\text{A}\beta(1-42)}$  tetramer 3D structure (PDB code 6RHY) where the amide protons of the affected residues are represented as red spheres (Figure 4B). The affected residues showed to be close in space and defined a specific binding site within the tetramer structure. These CSPs were used to perform driven docking of SST14 with the  $\beta\text{PFO}_{\text{A}\beta(1-42)}$  tetramer structure using the high ambiguity driven docking approach (HADDOCK).<sup>34</sup> The best-scoring structural clusters that we obtained suggested a binding mode of SST14 in the  $\beta\text{PFO}_{\text{A}\beta(1-42)}$  tetramer where the peptide interacted with the flexible edges of the tetramer and interestingly also tightly with the alpha helix of the green subunit (Figure 4C).

The binding site defined in our study, enabled us to rationalize the specificity of the interaction between both entities since the spatial distribution of the residues in the  $\beta\text{PFO}_{\text{A}\beta(1-42)}$  tetramer is completely different to that of monomeric  $\text{A}\beta(1-42)$ . The localization of the site was also in accordance with the 2:1 stoichiometry of the binding observed by ITC and native MS. Indeed, the symmetric topology of the tetramer contains two possible binding sites in the superior and inferior flexible ends that are solvent-exposed and thus, accessible to SST14.



## Discussion

In summary, our findings show that SST14 binds to  $\beta$ PFO<sub>A $\beta$ (1-42)</sub> tetramers with an affinity in the low micromolar range. Native MS experiments prove the binding to be specific for this oligomeric form with a 2:1 (SST14 to  $\beta$ PFO<sub>A $\beta$ (1-42)</sub> tetramer) stoichiometry, in accordance with ITC data. Our NMR experiments reveal two symmetric binding sites near the flexible ends of the tetramer. Restraint-driven *in silico* docking enables us to propose a binding mode of SST14 to the tetramer structure. Altogether, we conclude that SST14, an *in vivo* binder to A $\beta$  oligomers,<sup>18</sup> specifically binds to  $\beta$ PFO<sub>A $\beta$ (1-42)</sub> tetramer.

We observed an important difference when comparing our results with previously reported work on the binding of SST14 to soluble oligomers of A $\beta$ (1-42).<sup>18</sup> Indeed, work by Schmitt-Ulms and collaborators postulated that SST14 did not bind to A $\beta$ (17-42) oligomers which led them to conclude that the N-terminus was involved in the binding site. Our data, on the contrary, suggests that residues 18-29 are mainly involved in the binding with special emphasis on the ones forming the short alpha helix, residues L17 to F20. We recently showed that while A $\beta$ (1-42) incorporates both as the orange and green subunit in the  $\beta$ PFO<sub>A $\beta$ (1-42)</sub> tetramer arrangement, A $\beta$ (17-42) only incorporates as the green subunit,<sup>17</sup> which prevents A $\beta$ (17-42) to form  $\beta$ PFO<sub>A $\beta$ (1-42)</sub> tetramer by itself. Thus, for  $\beta$ PFO<sub>A $\beta$ (1-42)</sub> tetramer to form it is required that at least 50% of the peptides contain the N-terminus. These results evidence that using shortened versions of proteins can have a huge impact in protein self-assembly and structure. Moreover, work by Schmitt-Ulms *et al.* was performed on soluble oligomers while ours on a membrane-associated oligomer. Therefore, the binding to SST14 may be different for each oligomer type. The authors also emphasized the importance of W8 of SST14 for the binding to occur. Indeed, this residue has been described to play an important role in the activity of the peptide when binding SSTRs.<sup>35</sup>

Whilst our CSP-driven docking did not converge to a singular configuration for the SST14:  $\beta$ PFO<sub>A $\beta$ (1-42)</sub> tetramer interaction, a frequent observation across the best performing poses was that SST14 docks into the concave interior at the solvent-exposed edges of the  $\beta$ PFO<sub>A $\beta$ (1-42)</sub> tetramer (Figure 4C, Figure S5). In many of our calculated models, W8 of SST14 was found to interact with the hydrophobic residues of the  $\beta$ PFO<sub>A $\beta$ (1-42)</sub> tetramer, suggesting that W8 of SST14 could possibly mediate an interaction with the membrane-associated A $\beta$ (1-42) tetramer.

In the AD context, the critical role of SST14 in the metabolism of A $\beta$ (1-42) through the regulation of neprilysin<sup>23</sup> inevitably points towards the potential degradation of oligomeric forms of A $\beta$ (1-42). Two important conclusions of the work by Saido and collaborators are the location of the SST14-neprilysin interaction situated near or in the cellular membrane and the fact that somatostatin-regulated neprilysin activity selectively depleted A $\beta$ (1-42) but not A $\beta$ (1-40). Interestingly, the aforementioned facts also apply to  $\beta$ PFO<sub>A $\beta$ (1-42)</sub> tetramer since it is able to incorporate into membranes<sup>17</sup> and is exclusively formed by A $\beta$ (1-42) but not A $\beta$ (1-40).<sup>16</sup> Proteolytic activities are tightly controlled biological processes that can be regulated at different levels such as through the formation of an activation complex.<sup>36</sup> Therefore, we cannot exclude that binding of SST14 to the  $\beta$ PFO<sub>A $\beta$ (1-42)</sub> tetramer could induce its degradation.

In the present study, we show at a structural level how SST14, which has been reported to bind to A $\beta$  oligomers in human brain extracts, also binds to  $\beta$ PFO<sub>A $\beta$ (1-42)</sub> tetramer. We think these results strengthen the relation of SST14 with the amyloid cascade and due to the clear implication of SST14 in AD, it positions  $\beta$ PFO<sub>A $\beta$ (1-42)</sub> tetramer as relevant oligomer form of A $\beta$  and as a potential target for AD.

## **Acknowledgement**

This study was supported by Spanish Ministry of Economy, Industry and Competitiveness (MINECO, SAF2015-68789 to N.C. and CTQ2017-87840-P to A.R.), the Fondation Recherche Médicale (AJE20151234751) and the Conseil Régional d'Aquitaine Limousin Poitou-Charentes (1R30117-00007559). E.P. was a Ph.D. fellow funded by MINECO (FPI). We thank institutional funding from MINECO through the Centres of Excellence Severo Ochoa Award, and IRB Barcelona through the CERCA Programme of the Catalan Government. We acknowledge Mass Spectrometry and Proteomics Core Facility of IRB Barcelona, the NMR facility at IECB and Cameron Mackereth for his help with the ITC experiments and analysis.

## **Competing Interests**

The authors declare no competing financial interests.

## References

- (1) Hardy, J. A., and Higgins, G. A. (1992) Alzheimer's disease: the amyloid cascade hypothesis. *Science* 256, 184–185.
- (2) Selkoe, D. J., and Hardy, J. (2016) The amyloid hypothesis of Alzheimer's disease at 25 years. *EMBO Mol Med* 8, 595–608.
- (3) Kimberly, W. T., LaVoie, M. J., Ostaszewski, B. L., Ye, W., Wolfe, M. S., and Selkoe, D. J. (2003) Gamma-secretase is a membrane protein complex comprised of presenilin, nicastrin, Aph-1, and Pen-2. *Proc. Natl. Acad. Sci. U.S.A.* 100, 6382–6387.
- (4) Haass, C., and Selkoe, D. J. (2007) Soluble protein oligomers in neurodegeneration: lessons from the Alzheimer's amyloid beta-peptide. *Nat. Rev. Mol. Cell Biol.* 8, 101–112.
- (5) Xiao, Y., Ma, B., McElheny, D., Parthasarathy, S., Long, F., Hoshi, M., Nussinov, R., and Ishii, Y. (2015) A $\beta$ (1–42) fibril structure illuminates self-recognition and replication of amyloid in Alzheimer's disease. *Nat. Struct. Mol. Biol.* 22, 499–505.
- (6) Wälti, M. A., Ravotti, F., Arai, H., Glabe, C. G., Wall, J. S., Böckmann, A., Güntert, P., Meier, B. H., and Riek, R. (2016) Atomic-resolution structure of a disease-relevant A $\beta$ (1–42) amyloid fibril. *Proc. Natl. Acad. Sci. U.S.A.* 113, E4976–E4984.
- (7) Colvin, M. T., Silvers, R., Ni, Q. Z., Can, T. V., Sergeev, I., Rosay, M., Donovan, K. J., Michael, B., Wall, J., Linse, S., and Griffin, R. G. (2016) Atomic Resolution Structure of Monomorphic A $\beta$  42 Amyloid Fibrils. *J. Am. Chem. Soc.* 138, 9663–9674.
- (8) Gremer, L., Schölzel, D., Schenk, C., Reinartz, E., Labahn, J., Ravelli, R. B. G., Tusche, M., Lopez-Iglesias, C., Hoyer, W., Heise, H., Willbold, D., and Schröder, G. F. (2017) Fibril structure of amyloid- $\beta$ (1–42) by cryo-electron microscopy. *Science* 358, 116–119.
- (9) Barrett, P. J., Song, Y., Van Horn, W. D., Hustedt, E. J., Schafer, J. M., Hadziselimovic, A., Beel, A. J., and Sanders, C. R. (2012) The amyloid precursor protein has a flexible transmembrane domain and binds cholesterol. *Science* 336, 1168–1171.
- (10) Arispe, N., Rojas, E., and Pollard, H. B. (1993) Alzheimer disease amyloid beta protein forms calcium channels in bilayer membranes: blockade by tromethamine and aluminum. *Proc. Natl. Acad. Sci. U.S.A.* 90, 567–571.
- (11) Butterfield, S. M., and Lashuel, H. A. (2010) Amyloidogenic protein-membrane interactions: mechanistic insight from model systems. *Angew. Chem. Int. Ed. Engl.* 49, 5628–5654.
- (12) Kaye, R., Sokolov, Y., Edmonds, B., McIntire, T. M., Milton, S. C., Hall, J. E., and Glabe, C. G. (2004) Permeabilization of lipid bilayers is a common conformation-dependent activity of soluble amyloid oligomers in protein misfolding diseases. *J. Biol. Chem.* 279, 46363–46366.
- (13) Hirakura, Y., Lin, M. C., and Kagan, B. L. (1999) Alzheimer amyloid abeta1-42 channels: effects of solvent, pH, and Congo Red. *J. Neurosci. Res.* 57, 458–466.
- (14) Bode, D. C., Baker, M. D., and Viles, J. H. (2017) Ion Channel Formation by Amyloid- $\beta$ 42 Oligomers but Not Amyloid- $\beta$ 40 in Cellular Membranes. *J. Biol. Chem.* 292, 1404–1413.
- (15) Bode, D. C., Freeley, M., Nield, J., Palma, M., and Viles, J. H. (2019) Amyloid- $\beta$  oligomers have a profound detergent-like effect on lipid membrane bilayers, imaged by atomic force and electron microscopy. *J. Biol. Chem.* 294, 7566–7572.

- (16) Serra-Batiste, M., Ninot-Pedrosa, M., Bayoumi, M., Gairí, M., Maglia, G., and Carulla, N. (2016) A $\beta$ 42 assembles into specific  $\beta$ -barrel pore-forming oligomers in membrane-mimicking environments. *Proc. Natl. Acad. Sci. U.S.A.* 113, 10866–10871.
- (17) Ciudad, S., Puig, E., Botzanowski, T., Meigooni, M., Arango, A. S., Do, J., Mayzel, M., Bayoumi, M., Chaignepain, S., Maglia, G., Cianferani, S., Orekhov, V., Tajkhorshid, E., Bardiaux, B., and Carulla, N. (2020) A $\beta$ (1-42) tetramer and octamer structures reveal edge conductivity pores as a mechanism for membrane damage. *Nat Commun* 11, 3014.
- (18) Wang, H., Muiznieks, L. D., Ghosh, P., Williams, D., Solarski, M., Fang, A., Ruiz-Riquelme, A., Pomès, R., Watts, J. C., Chakrabarty, A., Wille, H., Sharpe, S., and Schmitt-Ulms, G. (2017) Somatostatin binds to the human amyloid  $\beta$  peptide and favors the formation of distinct oligomers. *Elife* 6, 561.
- (19) Reichlin, S. (1983) Somatostatin. *N. Engl. J. Med.* 309, 1495–1501.
- (20) Morisset, J. (2017) Somatostatin: One of the Rare Multifunctional Inhibitors of Mammalian Species. *Pancreas* 46, 8–18.
- (21) Davies, P., Katzman, R., and Terry, R. D. (1980) Reduced somatostatin-like immunoreactivity in cerebral cortex from cases of Alzheimer disease and Alzheimer senile dementia. *Nature* 288, 279–280.
- (22) Hayashi, M., Yamashita, A., and Shimizu, K. (2011) Somatostatin and brain-derived neurotrophic factor mRNA expression in the primate brain: decreased levels of mRNAs during aging. *Brain Research* 749, 283–289.
- (23) Saito, T., Iwata, N., Tsubuki, S., Takaki, Y., Takano, J., Huang, S.-M., Suemoto, T., Higuchi, M., and Saido, T. C. (2005) Somatostatin regulates brain amyloid  $\beta$  peptide A $\beta$ 42 through modulation of proteolytic degradation. *Nat. Med.* 11, 434–439.
- (24) Duron, E., Vidal, J.-S., Grousselle, D., Gabelle, A., Lehmann, S., Pasquier, F., Bombois, S., Buée, L., Allinquant, B., Schraen-Maschke, S., Baret, C., Rigaud, A.-S., Hanon, O., and Epelbaum, J. (2018) Somatostatin and Neuropeptide Y in Cerebrospinal Fluid: Correlations With Amyloid Peptides A $\beta$ 1-42 and Tau Proteins in Elderly Patients With Mild Cognitive Impairment. *Front Aging Neurosci* 10, 297.
- (25) Rasmussen, S. G. F., DeVree, B. T., Zou, Y., Kruse, A. C., Chung, K. Y., Kobilka, T. S., Thian, F. S., Chae, P. S., Pardon, E., Calinski, D., Mathiesen, J. M., Shah, S. T. A., Lyons, J. A., Caffrey, M., Gellman, S. H., Steyaert, J., Skiniotis, G., Weis, W. I., Sunahara, R. K., and Kobilka, B. K. (2011) Crystal structure of the  $\beta$ 2 adrenergic receptor-Gs protein complex. *Nature* 477, 549–555.
- (26) Bianchi, M., Turner, H. L., Nogal, B., Cottrell, C. A., Oyen, D., Pauthner, M., Bastidas, R., Nedellec, R., McCoy, L. E., Wilson, I. A., Burton, D. R., Ward, A. B., and Hangartner, L. (2018) Electron-Microscopy-Based Epitope Mapping Defines Specificities of Polyclonal Antibodies Elicited during HIV-1 BG505 Envelope Trimer Immunization. *Immunity* 49, 288–300.e8.
- (27) Bai, Y. (2015) Detecting protein-protein interactions by gel filtration chromatography. *Methods Mol. Biol.* 1278, 223–232.
- (28) Anoop, A., Ranganathan, S., Dhaked, Das, B., Jha, N. N., Pratihari, S., Ghosh, S., Sahay, S., Kumar, S., Das, S., Kombrabail, M., Agarwal, K., Jacob, R. S., Singru, P., Bhaumik, P., Padinhateeri, R., Kumar, A., and Maji, S. K. (2014) Elucidating the role of disulfide bond on amyloid formation and fibril reversibility of somatostatin-14: relevance to its storage and secretion. *J. Biol. Chem.* 289, 16884–16903.
- (29) Laganowsky, A., Reading, E., Hopper, J. T. S., and Robinson, C. V. (2013) Mass spectrometry of intact membrane protein complexes. *Nat Protoc* 8, 639–651.
- (30) Gupta, K., Donlan, J. A. C., Hopper, J. T. S., Uzdavinys, P., Landreh, M., Struwe, W. B., Drew, D., Baldwin, A. J., Stansfeld, P. J., and Robinson, C. V. (2017) The role of interfacial lipids in stabilizing membrane protein oligomers. *Nature* 541, 421–424.

- (31) Reading, E., Liko, I., Allison, T. M., Benesch, J. L. P., Laganowsky, A., and Robinson, C. V. (2015) The role of the detergent micelle in preserving the structure of membrane proteins in the gas phase. *Angew. Chem. Int. Ed. Engl.* 54, 4577–4581.
- (32) Williamson, M. P. (2013) Using chemical shift perturbation to characterise ligand binding. *Prog Nucl Magn Reson Spectrosc* 73, 1–16.
- (33) Furukawa, A., Konuma, T., Yanaka, S., and Sugase, K. (2016) Quantitative analysis of protein-ligand interactions by NMR. *Prog Nucl Magn Reson Spectrosc* 96, 47–57.
- (34) Dominguez, C., Boelens, R., and Bonvin, A. M. J. J. (2003) HADDOCK: a protein-protein docking approach based on biochemical or biophysical information. *J. Am. Chem. Soc.* 125, 1731–1737.
- (35) Veber, D. F., Holly, F. W., Paleveda, W. J., Nutt, R. F., Bergstrand, S. J., Torchiana, M., Glitzer, M. S., Saperstein, R., and Hirschmann, R. (1978) Conformationally restricted bicyclic analogs of somatostatin. *Proc. Natl. Acad. Sci. U.S.A.* 75, 2636–2640.
- (36) Turk, B. (2006) Targeting proteases: successes, failures and future prospects. *Nat Rev Drug Discov* 5, 785–799.

## Figures and Figure Legends

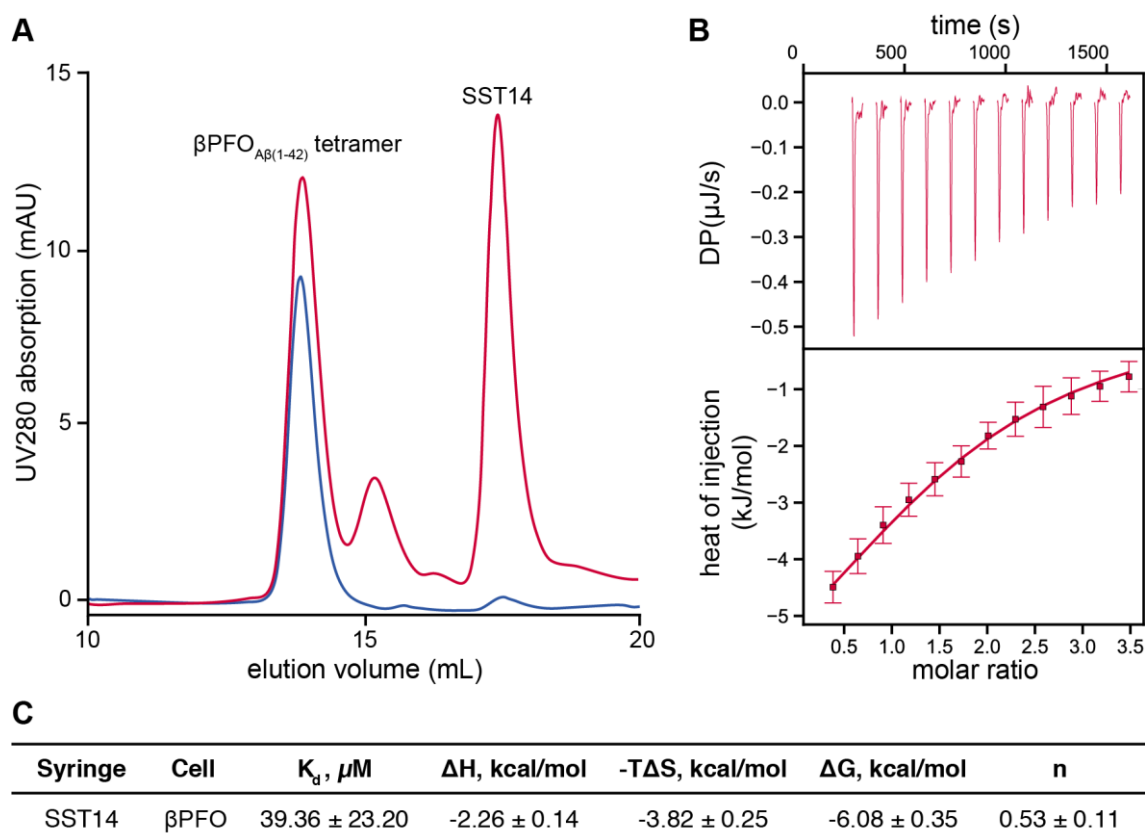


**Figure 1.** SST14 binding to  $\beta\text{PFO}_{\text{A}\beta(1-42)}$  tetramer assessed by SEC and ITC. (A) SEC elution profile for  $\beta\text{PFO}_{\text{A}\beta(1-42)}$  tetramer after 24 hours of its formation in the absence (blue) and in the presence of SST14 (red). The peaks have been labeled with the elution volume of  $\beta\text{PFO}_{\text{A}\beta(1-42)}$  tetramer and SST14. (B) ITC thermogram (top) and analysis of the fitted binding isotherm (bottom) for  $\beta\text{PFO}_{\text{A}\beta(1-42)}$  tetramer titrated with SST14. Standard deviation values were obtained from three independent replicates. (C) Thermodynamic binding parameters of the interaction determined from ITC experiments at 25°C and pH 9.0.

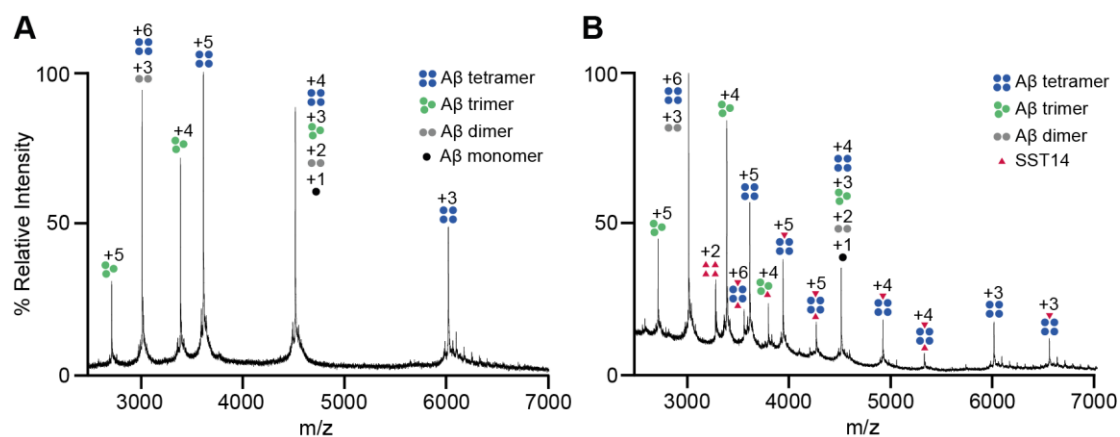


**Figure 2.** SST14 binding to  $\beta$ PFO<sub>A $\beta$ (1-42)</sub> tetramer assessed by native MS. (A) Electrospray ionization MS (ESI-MS) spectrum of  $\beta$ PFO<sub>A $\beta$ (1-42)</sub> tetramer (150  $\mu$ M A $\beta$ (1-42), 7.2 mM LDAO, 200 mM Ammonium Carbonate, pH 9.0 incubated for 24 hours). (B) ESI-MS spectrum of  $\beta$ PFO<sub>A $\beta$ (1-42)</sub> tetramer coincubated with SST14 (150  $\mu$ M A $\beta$ 42, 150  $\mu$ M SST14, 7.2 mM LDAO, 200 mM Ammonium Carbonate, pH 9.0 incubated for 24 hours). Charge states corresponding to SST14; A $\beta$ (1-42) monomer, dimer, trimer, and tetramer are indicated with schematic drawings and labelled, respectively, in red, black, grey, green, and blue.



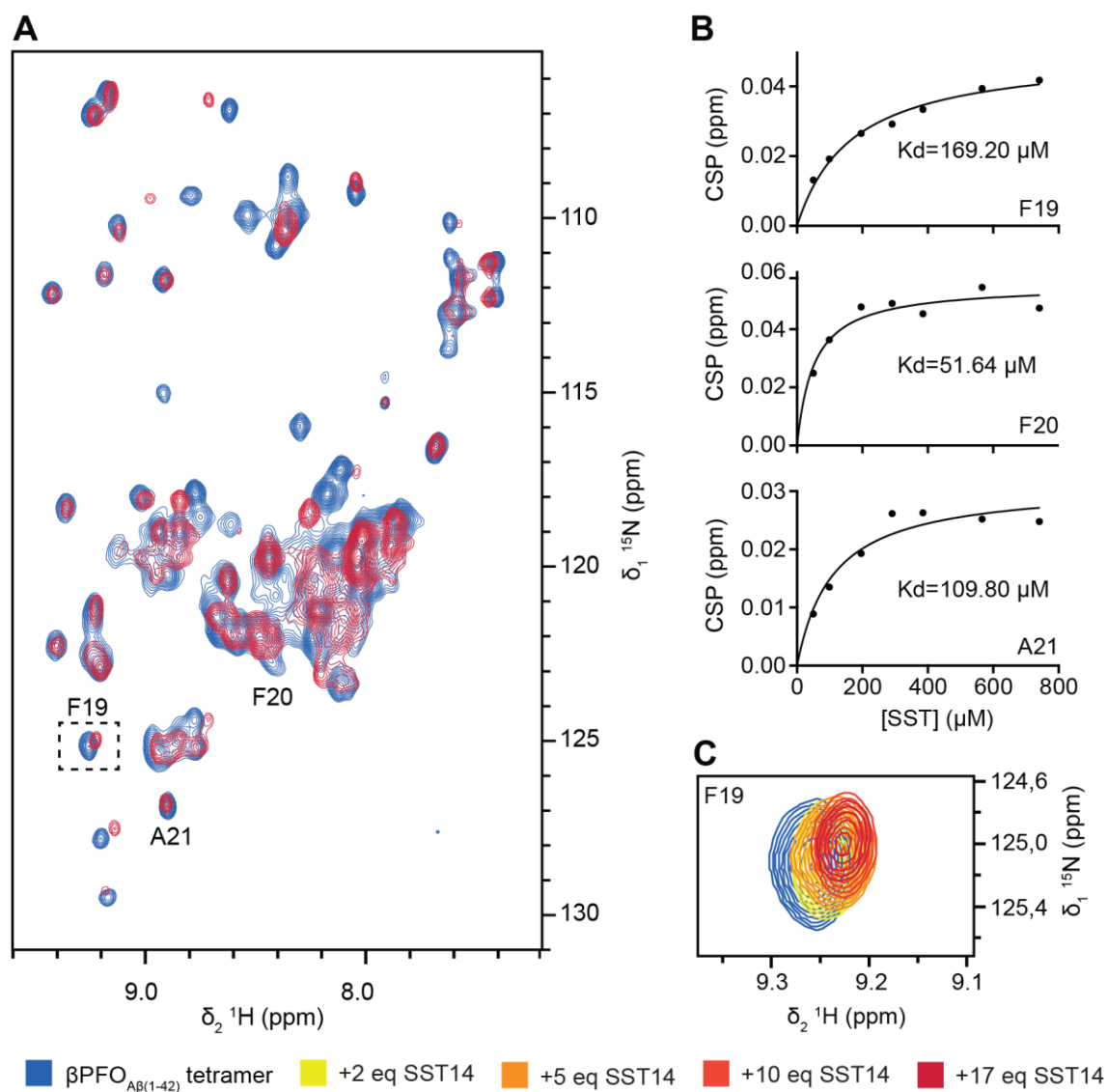


**Figure 3.** NMR titration of SST14 to  $\beta$ PFO<sub>AB(1-42)</sub> tetramer. (A) Two-dimensional [<sup>15</sup>N, <sup>1</sup>H]-SOFAST-HMQC spectra of  $\beta$ PFO<sub>AB(1-42)</sub> tetramer (230  $\mu$ M A $\beta$ (1-42), 7.71 mM d<sub>38</sub>-DPC, 10 mM d<sub>12</sub>-Tris·DCl, pH 8.5) alone (blue) and in the presence of 17 equivalents of SST14 (red). (B) Fitted saturation curves of residues F19, F20 and A21 during SST14 titration with their respective calculated  $K_D$ . (C) Close-up view of residue F19 from the titration in the presence of 0 (blue), 2 (yellow), 5 (orange), 10 (coral) and 17 (red) equivalents (eq.) of SST14.

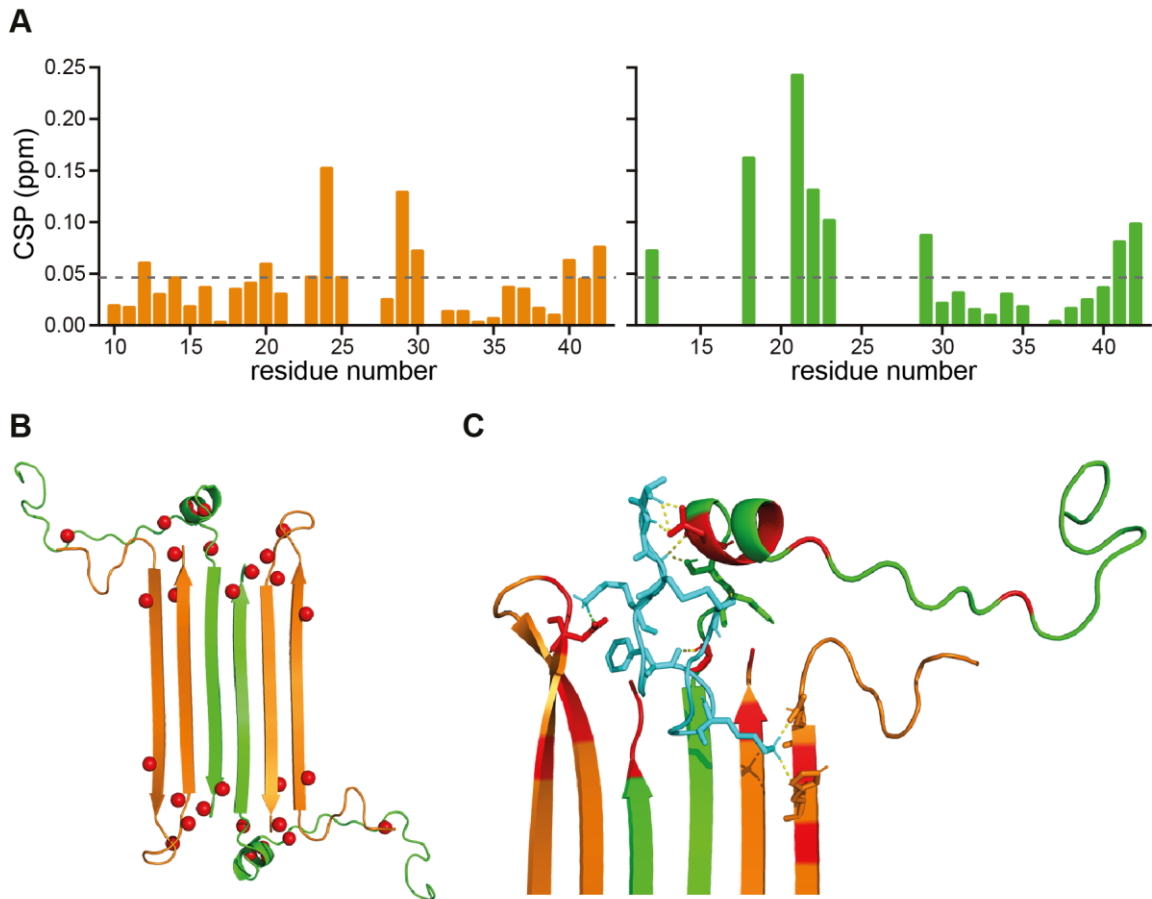


**Figure 4.** Binding site of SST14 to  $\beta$ PFO<sub>A $\beta$ (1-42)</sub> tetramer. (A) Representation of the CSP of the residues within the orange and green subunits of the  $\beta$ PFO<sub>A $\beta$ (1-42)</sub> tetramer induced by the presence of SST14. The grey dashed line indicates the threshold dictated by the standard deviation ( $\sigma$ ). Source data are provided in Source data 1. (B) Representation of the residues affected by chemical shift changes (red spheres) in the presence of SST14 within the 3D structure of the  $\beta$ PFO<sub>A $\beta$ (1-42)</sub> tetramer (PDB code 6RHY). (C) Best-ranked structure proposing a binding mode of SST14 (cyan, PDB code 2MI1) with  $\beta$ PFO<sub>A $\beta$ (1-42)</sub> tetramer (orange and green). Residues introduced as ambiguous interaction restraints (AIRs) are colored in red.